

Funari V.; Mantovani L.; Vigliotti L.; Tribaudino M.; Dinelli E.; Braga R

Superparamagnetic iron oxides nanoparticles from municipal solid waste incinerators

Science of the Total Environment 2018;

Revised copy

1 **ABSTRACT**

2 During their production, management, and landfilling, bottom (BA) and fly (FA) ashes from
3 municipal solid waste incineration may liberate Fe-bearing, ultrafine particles and easily enter
4 different environmental sinks of the biosphere. We aim to explore a collection of BA and FA
5 samples from Italian incinerators to probe magnetic mineralogy and the fraction of harmful
6 superparamagnetic (SP) nanoparticles ($d < 30$ nm). X-ray diffraction, electron microscopy
7 observation, temperature- and frequency-dependent magnetometry, and Mossbauer analysis are
8 performed. The integration of information from our rock magnetic and non-magnetic techniques
9 leads us to conclude that the dominant magnetic carrier in our samples is magnetite and its
10 intermediate/impure forms, while sulphides (i.e., monoclinic pyrrhotite) are important ancillary
11 magnetic phases. The SP fraction fluxing from the BA and FA outputs of a single incinerator is
12 detected and estimated in 10^3 tons/year. This work stresses the need to calibrate the current
13 technologies towards a safer management of combustion ashes and certainly to inform the
14 environmental impact assessment by using a combination of different methods.

15 **1. INTRODUCTION**

16 Human exposure to nanoparticles pollution and environmental contamination related to Fe-
17 bearing phases has dramatically increased during the last 30 years. It is estimated that million tons
18 of toxic pollutants are released into the air each year [1]. Amongst these pollutants, iron- and
19 sulphur-rich nanoparticles are liable of a range of adverse health effects in the general population,
20 from subclinical chronic diseases to premature death [2]. Magnetite nanoparticles from particulate
21 matter are also found in human brain suggesting a connection between the presence of these
22 particles and neurodegenerative diseases such as Alzheimer's disease [3]. In this context,
23 environmental magnetic studies are beneficial to explore environmental media and characterise
24 therein contained iron minerals according to ferrimagnetic or antiferromagnetic properties [4].
25 Magnetic minerals can act as pollutant carriers through adsorption and structural incorporation.
26 Some studies reported a correlation between magnetic parameters and heavy metal contents in
27 different kinds of material, such as airborne particulate matter [5, 6], roadside pollution [7, 8], soils
28 [9-12] lake and river sediments [13, 14], and fly ashes [15-18]. Magnetic parameters are
29 successfully used as a tracer of a wide range of pollutants related to anthropogenic activities and
30 also to detect particulates that strictly represent a respiratory hazard. Magnetic properties are highly
31 sensitive to certain particle size ranges; conventional grain-size assignments (for magnetite) are:

32 superparamagnetic (SP: $d < 30 \text{ nm}$); stable single domain (SD: $30 \text{ nm} < d < 84 \text{ nm}$); pseudo-single
33 domain (PSD: $84 \text{ nm} < d < 17 \text{ }\mu\text{m}$); multi-domain (MD: $d > 17 \text{ }\mu\text{m}$) [19]. Particles formed by
34 combustion sources are usually fine or ultrafine [20], with a diameter in the submicron range, and
35 have the highest potential to endanger life [20, 21]. Heavy metal concentrations in the fine
36 particulate were found to be higher in industrial districts than in other areas [7], emphasising the
37 health risk associated with industrial emitters and industrial processes. The particles diameter and
38 the size distributions can vary in space and time due to differences in emission sources and
39 atmospheric processes [22, 23]. Therefore, dust and the finest fraction of ashes generated by
40 industrial processes gain increasing attention in environmental magnetic studies aimed to assess
41 anthropogenic alterations of air, soil, and water. Since coal combustion represents an important
42 world source of energy supply leading to the production of waste and dust, the iron minerals
43 occurring in raw materials, fuels, additives, or residues are carefully studied. During such a
44 technological process, the iron minerals are acknowledged to form highly magnetic particles with
45 the tendency to bind hazardous elements. An extensive literature on fly ashes and polluted soils
46 from coal-combustion power plants is available [15-18, 24]. Some works on Fe-smelters [14] and
47 on municipal landfill leachates [25] do exist. However, the assessment of the magnetic behaviour of
48 municipal solid waste incineration (MSWI) ashes remains largely overlooked despite their
49 recognised hazardous nature and the nanoparticles emission is acknowledged to occur [26]. The
50 municipal solid waste incineration (MSWI) is considered a good practice for reducing the waste
51 volume and recovering its energy to produce electricity. Nevertheless, the risk perceived by people
52 living near waste incinerators is very high and testified by a diffuse social response like the “*not in*
53 *my backyard*”. MSWI plants generate huge amounts of solid residues, around 10^4 t/a [27], and ca.
54 0.7 tons of gases and particulate vapour per tonne of input waste [28]. The bottom ash (BA) is the
55 largest fraction generated in the combustion chamber; after an approximate residence time of 30 to
56 45 minutes on the grate furnace (up to 1150° C), the BA is usually quenched in cold water.
57 Conversely, the particulate material from the combustion chamber is sparged to the Air Pollution
58 Control (APC) system equipped with some flue gas treatments devices, such as scrubbers, bag
59 filters, and electrostatic precipitators. Both MSWI ashes and MSWI emission at the stacks showed
60 particle diameters of recognised inhalable risk [26, 29], encompassing the risk of primary and
61 secondary pollution. The contribution of waste incinerators to the intake fraction is thought to be
62 negligible [30], but the limited number of studies coupled with the lack of standard protocols for the
63 risk assessment emphasises the need to further investigation.

64 This work aims at:

- 65 • investigating the magnetic properties of MSWI ashes from four Italian facilities;
- 66 • identifying the magnetic components liable of the strong magnetic signals observed in
- 67 prior start-point measurements [27, 31];
- 68 • evaluating whether a new pollution risk related to SP grains is significant.

69 Spatiotemporal variations of MSWI pollution patterns are not assessed in this work. Here we
70 provide magnetic reference data of a particular combustion product to inform pollution-related
71 environmental magnetic studies and to assess potential health risks triggered by urban waste
72 incineration.

73 **2. SAMPLES AND METHODS**

74 A collection of BA and FA samples was taken from four MSWI systems of northern Italy
75 following the sampling methodology as in Funari et al. [32]. The selected facilities are located in
76 four different municipalities and serve an area of about 10000 km² within the Po Valley. Each
77 incinerator equipped with a grate-furnace system operates at temperatures between 850-1100° C.
78 The solid waste input, which averages $1.5 \cdot 10^5$ tons per year, consists of 90% household waste and
79 10% of special waste, i.e. processing waste from steel-making industries, scraps from ceramics,
80 automobile shredder residues, and hospital/pharmaceutical waste. The solid waste output averages
81 $4.6 \cdot 10^4$ BA and $4.1 \cdot 10^3$ FA tons per year, respectively. The figure for BA does not include the
82 ferrous metal scraps (ranging $5-8 \cdot 10^3$ tons per year) that are recovered by a rough magnetic
83 separation after quenching and re-melted for reuse in an integrated system; the ferrous metal
84 fraction is not taken in this study. The FA samples are further divided into different categories
85 depending on the APC technology. Where it was possible, FA were collected at the first recovery
86 phase without any treatment (untreated, FAU), after the electrostatic precipitator (FAE), and after
87 chemical bag filters, which involved the use of soda (FAS) or lime (FAL) additives. It is recognised
88 that samples of incinerated wastes cannot display the variability inherent in a given plant during the
89 time and changes of the feedstock materials. Nevertheless, each sample is representative of the
90 MSWI ash category of each MSWI plant, as determined by previous works focusing on the same
91 materials [27, 32, 33].

92 We analysed BA and FA samples by a range of magnetic and mineralogical techniques. The
93 collected materials were oven dried at 40° C for one week. The biggest metallic fragments partially
94 melted or destroyed by the thermal treatment ($d > 1$ cm; mostly in BA samples) were hand-sorted
95 and removed before the measurements. For samples with abundant magnetic materials (i.e., BA),

96 magnetic extracts from dried and milled samples were obtained using a Nd hand magnet with a
97 plastic sleeve. Extracts from samples with sparse magnetic materials (i.e., FA), were collected using
98 a Frantz magnetic separator by imparting a 1.1 A current in the laminar isodynamic region and a
99 +15° side slope of the chute. A range of magnetic measurements was conducted on triplicate
100 samples at the Institute of Marine Sciences of the National Research Centre (CNR-ISMAR,
101 Bologna) and the Institute for Rock Magnetism (IRM, University of Minnesota). The chemical
102 composition, mineralogy, and morphology were investigated by non-magnetic technique, such as
103 XRF, SEM, XRD, at the BiGeA Department (University of Bologna) and the Department of
104 Physics and Earth Sciences (University of Parma). Furthermore, ⁵⁷Fe Mössbauer spectra were
105 measured at the IRM (University of Minnesota) on selected original samples and magnetic extracts.
106 Further details on analytical methods are in the Supporting Information (SI).

107 **3. RESULTS AND DISCUSSION**

108 ***3.1 XRD analysis and morphological observations***

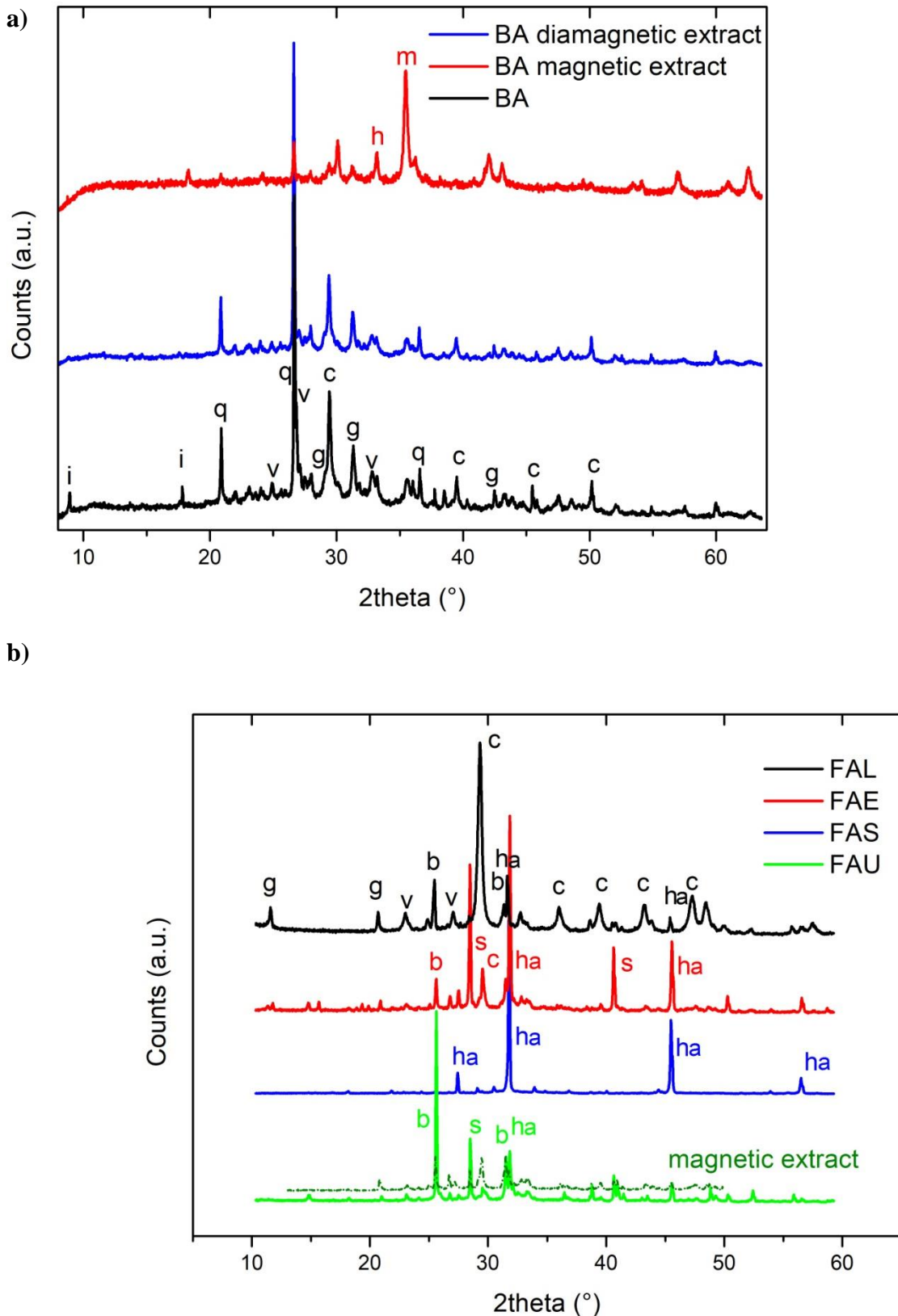
109 The BA and FA samples show complex X-ray diffraction patterns (Fig. 1), consisting of
110 crystalline phases and large amounts of amorphous/nanocrystalline materials. According to
111 numerous studies, the main phases in BA consists of solid phases with high melting points already
112 contained in the municipal solid waste feed and melt products such as glass, melitite- and spinel-
113 group minerals [34, 35]. Conversely, FA have a quite different mineralogy ascribed to the MSWI
114 technological process from the combustion to the subsequent flue-gas cleaning, i.e. vaporisation,
115 melting, crystallisation, vitrification, condensation and precipitation [36]. The main crystalline
116 phases are sulphates, carbonates, chlorides silicates, phosphates, and oxides. The phases identified
117 by XRD analysis and their semi-quantitative estimates are reported in Table S.1. On the XRD
118 analysis, the iron oxides result in lower amounts compared to other minerals. The XRD patterns for
119 all our specimens show a considerable amount of amorphous or nanocrystalline materials, which is
120 estimated around 50 wt. % BA and 15-20 wt. % FA (see SI for details).

121 Among the crystalline phases in BA samples, a few minerals such as quartz, gehlenite and
122 calcium carbonates (both calcite and vaterite) are easily identified (Fig. 1a). Other mineral phases
123 cannot be identified by a simple search-matching procedure due to a large number of overlapping
124 peaks and to the shift of peaks position because of solid solution members. For example, the
125 presence of plagioclase, feldspar, and pyroxene in BA is highly probable but estimating their
126 chemical composition is unrealistic due to solid solutions and substitutions of other metal ions in

127 the crystal lattice. Phyllosilicates (e.g., muscovite, illite), iron oxides, and a few peaks identifying
128 metallic aluminium are detectable as minor phases. This mineralogical assemblage is characteristic
129 of all BA samples. The magnetic extract of BA shows the presence of iron oxides such as hematite,
130 magnetite and wüstite. It is important to stress that the X-ray pattern diffraction of magnetite is the
131 same of a large number of oxides with a spinel-structure like Ca/Mg-ferrite, hercynite, chromite,
132 titanomagnetite and so on. Chemical substitutions and solid solutions in the spinel mineral are very
133 common, signifying the possible presence of impure Fe^{2+} and Fe^{3+} oxides and iron vacancies.

134 Fig. 1b reports the XRD patterns of some FA categories, namely FAU, FAE, FAS and FAL
135 collected during different steps of filtration of the APC. All the FA have a lot of chlorides and
136 carbonates, whereas FAU, FAE and FAL also show a considerable amount of calcium sulphates,
137 both anhydrous and hydrated. Minor amounts of quartz and calcium alumina-silicates are also
138 detected. The FAS sample differs from FAU and FAE showing a large amount of NaCl, as a result
139 of the soda addition, and different mineralogical phases of carbonates (i.e., trona and nahcolite) and
140 sulphates (i.e., apththalite). Iron oxides are present in all FA samples, but they are relatively less
141 than those occurring in BA samples. The magnetic extract of the FAU sample doesn't help to
142 distinguish the magnetic mineral assemblage. As for BA, the presence of titanohematite or other
143 metals substituting in the spinel-like structures cannot be ruled out.

144 The SEM/EDS analysis on BA and FA (Fig. S.2) allows the observation of morphology and
145 grain-sizes, but the identification of potential substitutes/pollutants in the different mineral phases is
146 prevented. Both single crystals and glassy groundmass contain a significant amount of Si and Ca,
147 but also Fe, S, Ti, and other substituting/pollutant elements (e.g., Zn, Pb, etc.). Iron results in
148 association with Ca, Si, S, Ti, and other heavy metals. Some particles can be very small, with
149 diameters well below the micron range, overcoming the instrument resolution. Therefore: i)
150 pollutants may enter both crystalline and glassy phases, including those capable of a certain
151 magnetic response; ii) magnetic carriers are most probably minor phases, in form of impure oxides,
152 sulphates/sulphides (e.g., $\text{Fe}_2(\text{SO}_4)_3$, pyrrhotite, greigite), carbonates (e.g., siderite), alloys; iii) the
153 amorphous phase might be responsible for unaccounted magnetisation.



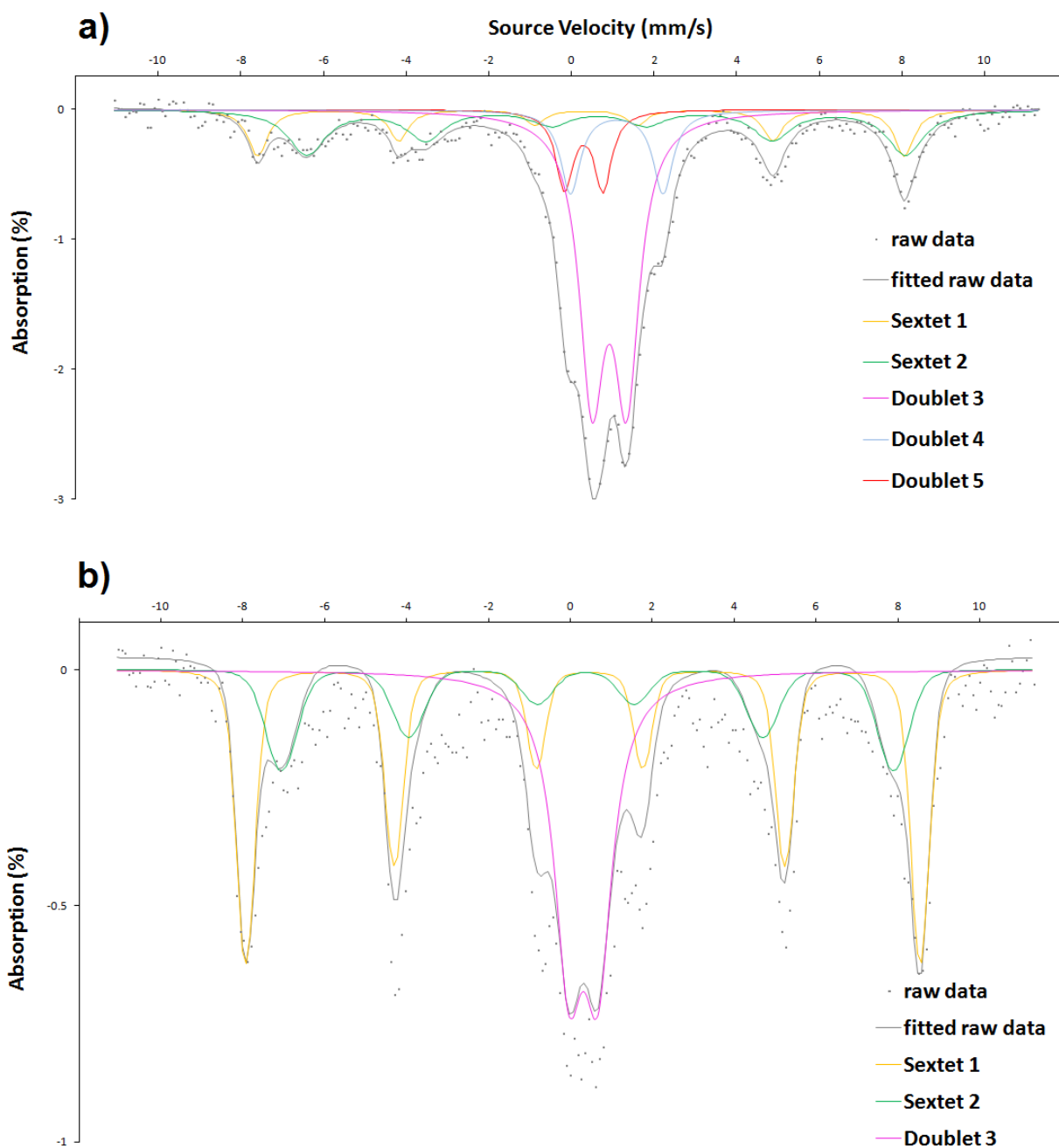
154 **Fig. 1** XRD spectra of representative samples of **a)** BA and **b)** different FA types, including magnetic
 155 extracts. For **a)**: *i* = illite, *q* = quartz, *v* = vaterite, *g* = gehlenite, *c* = calcite, *m* = magnetite, *h* =
 156 hematite; for **b)**: *g* = gypsum, *v* = vaterite, *b* = bassanite *c* = calcite, *ha* = halite, *s* = sylvite; FAL = bag
 157 filter fly ashes treated with lime; FAE = fly ashes from electrostatic precipitator; FAS = bag filter fly
 158 ashes treated with soda; FAU = untreated fly ashes.

159 3.2 Mössbauer spectroscopy

160 Mössbauer spectra (Fig. 2) and fitted parameters (Table S.2) for two selected samples of BA
161 and FA are reported. The Mössbauer spectrum of the FA sample has not displayed any signal, but
162 we were able to process the signal of a magnetic extract of the FA material. The obtained spectra of
163 BA and FA samples show considerable differences. In the BA sample (Fig. 2a), the sextets indicate
164 the two molecular geometries of magnetite (representing 34% of the whole spectrum) with their
165 characteristic parameters. However, the hyperfine field of Bhf for the sextets shows anomalies that
166 might relate to the presence of metallic iron, alloys, or magnetic sulphur minerals. The two central
167 doublets (i.e., 3 and 4 in Table S.2) with isomer shift close to 1 mm/s are characteristic of Fe²⁺ [37].
168 The high quadrupole splitting of doublets 3 and 4 might indicate either Al/Ti substitution in spinel-
169 like structures (i.e., FeAl₂O₄, TiFe₂O₄) or Fe²⁺ sulphides. The doublet 5 with a small isomer shift
170 may correspond to SP hematite, but the high quadrupole splitting might indicate Fe³⁺ ions in
171 carbonates/sulphates/silicates structures [5] as a superimposed signal. The FA sample (Fig. 2b) is
172 composed of two sextets with the characteristic Mössbauer parameters corresponding to magnetite.
173 The magnetite phase looks ferric (maghemitization) due to the low IS and cation substitution may
174 account for the observed low Bhf. The doublet 3 corresponds to a Fe³⁺ phase, but its large line
175 width (0.85 mm/s) most likely points to a superposition of, at least, two Fe³⁺ doublets which cannot
176 be resolved. Noteworthy, the FA sample produced the so-called “intermediate relaxation” effect due
177 to SP grains, which translates in a collapse of the sextet in favour of a paramagnetic doublet or
178 singlet. The signal from this phenomenon was removed prior to fitting, so any contribution from
179 that material is not in the fitted spectra and might have reduced the number of recognised doublets.
180 To a lesser extent, the BA sample displayed an intermediate relaxation effect that, however, was not
181 so high to force changes in the standard fitting procedure. The cations distribution deduced from
182 these measurements is the following: Fe³⁺ and Fe²⁺ ions account for ~32% and ~68%, respectively,
183 of the total iron atoms in the BA sample; for the FAU sample, almost all the iron atoms are Fe³⁺ and
184 only 7% Fe²⁺ ions. These estimates assume that magnetite is stoichiometric (i.e., that 2/3 of the total
185 Fe in magnetite is Fe³⁺ and 1/3 is Fe²⁺) and thus possible errors may derive from the assumption of
186 perfect stoichiometry.

187 Observed spectra and iron states in our samples markedly differ from data of coal fly ashes
188 [38, 39] and other anthropogenic dust from industrial emitters [18] as well as from urban
189 atmospheric particulate matter [5]. Conversely, the obtained spectra are similar to those reported
190 earlier by Fermo et al. [40] for a FAE sample collected from a MSWI plant that probably adopted a

191 similar incineration technology. Fermo and co-workers recognised hematite, but they had
192 difficulties in identifying other lines probably due to SP-related effects.

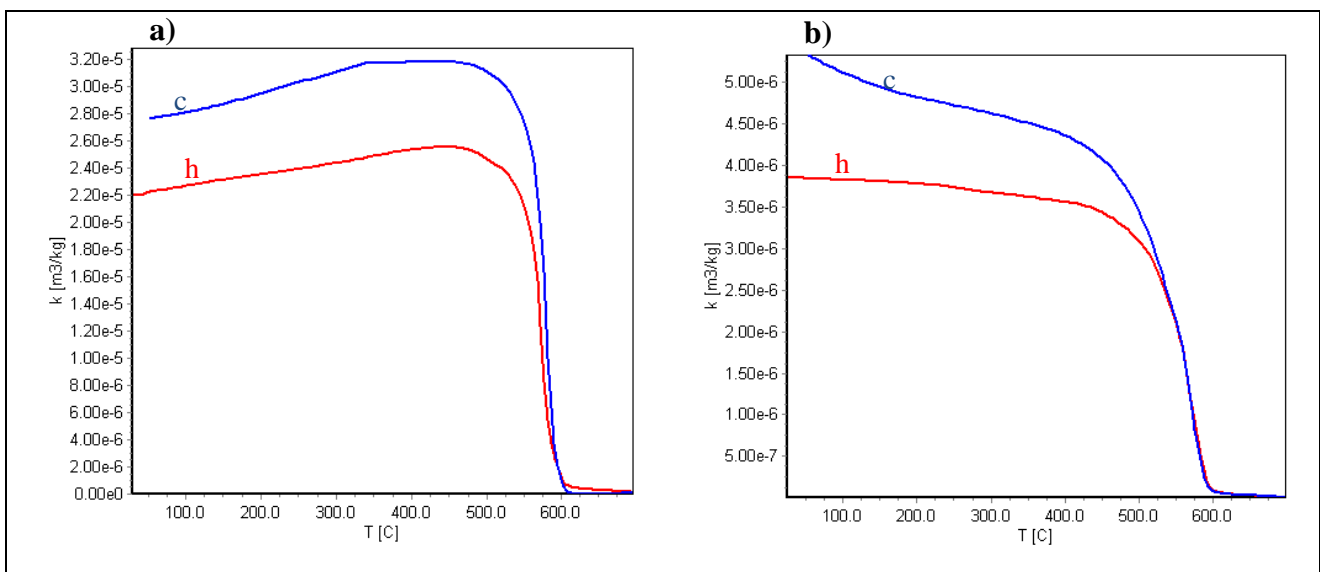


193

194 **Fig. 2** Mössbauer spectra of representative BA (a) and FA (b) samples, recorded at ~85 K. Deconvolution
195 fits using Lorentzian line shapes algorithm are provided. Fitting reliability can be assessed by comparing the
196 raw data points (dots). The spectrum in b results from a FAU magnetic extract since original material
197 produced a very weak signal. Further details on experimental conditions are provided in SI.

198 **3.3 Thermomagnetic analysis**

199 The analysis of the thermomagnetic curves of BA and FA samples indicates that magnetite
200 with its characteristic Curie temperature (T_C) of $\sim 580^\circ\text{C}$ is the main ferrimagnetic phase (Fig. 3).
201 The T_C of the FA sample (Fig. 3b) is slightly below 580°C likely due to a higher presence of
202 impure magnetite than in BA. The first derivative of the heating-cooling lines for the BA sample
203 also shows peaks at $\sim 300^\circ\text{C}$, unlike FA, that might represent the contribution of other carriers of
204 magnetic signal such as sulphides or native metals (e.g., Ni). In many cases, the first derivative of
205 the thermomagnetic curves for FA samples reveals a slight decrease of the heating curve near
206 temperatures between $500\text{--}550^\circ\text{C}$, which can be related to magnetite with a variable composition
207 (cation substitution). These peaks might reflect the presence of Ca/Mg-ferrite [18] that is likely
208 sourced from the lime/dolomite addition. Heating and cooling curves show that no significant
209 mineralogical changes occur during heating, while a certain proportion of weak magnetic minerals
210 may turn into stronger ones at high temperature, so susceptibility is higher during cooling. Evidence
211 of maghemitization is also found in BA samples in the first part (up to 500°C) of the
212 thermomagnetic lines where a susceptibility gain occurs (Fig. 3a). The hypothesis of a contribution
213 of maghemite transforming to hematite cannot be rejected especially in the BA sample, where the
214 susceptibility is not zero after 580°C . However, the diagnostic feature of maghemite (which T_C is
215 ca. 650°C) is not observed. During cooling of both samples, the magnetisation is almost completely
216 reversible until the T_C and then shows an increase in κ at the end of the run. Unlike the BA
217 thermomagnetic curves that display the characteristic shape of ferrimagnetic components, the
218 heating-cooling curves of all the FA samples reach the maximum of κ at room temperature. This
219 feature points to a contribution of paramagnetic phases that adds to the ferrimagnetic components.



220 **Fig. 3** Thermomagnetic curves of selected BA (a) and FA (b) samples in an air atmosphere. κ = magnetic
221 susceptibility, T = temperature, h = heating line, c = cooling line.

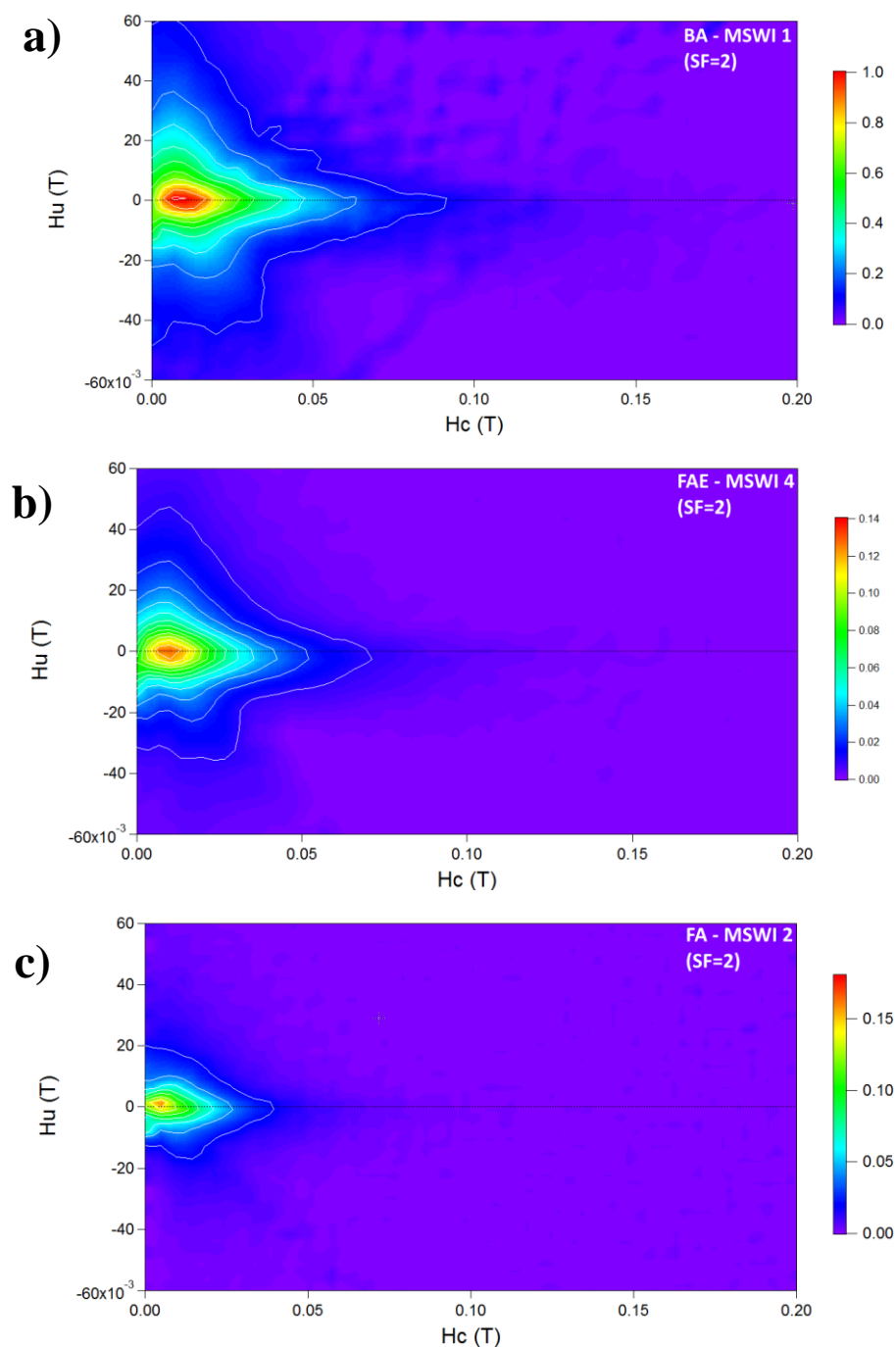
222 **3.4 Hysteresis properties**

223 The MSWI samples are characterised by narrow hysteresis curves (SI) that saturate below
224 ~200 mT and low coercivity (B_C range: 7.2 – 14.1 mT), indicating the predominant contribution of
225 low coercivity ferromagnetic minerals such as magnetite. Both MSWI samples produce tall, thin
226 hysteresis loops typical of pure magnetite with a significant reversible component of the
227 magnetisation [4]. The uncorrected loops (Fig. S.3) indicate a higher contribution of
228 paramagnetic/diamagnetic components in FA than in BA. Moreover, the hysteresis curves resemble
229 the typical loop of SP grains, showing a steep magnetisation versus field curve which saturates at
230 low fields [19]. Variations in grain-size play a major role in determining the shape of the curve [4];
231 we hypothesise that the shape of the overall loops is the combination of MD and SP magnetite
232 grains, with a larger contribution of pure MD magnetite in BA sample than in other FA [19]. The
233 BA samples show a slightly larger B_C than FA samples, averaging 10.5 mT and 8.6 mT,
234 respectively. The relatively high values of coercivity of remanence (B_{0CR}), ranging 24 – 52 mT,
235 confirm the presence of strong ferro(i)magnetic components. These differences in the mean values
236 of B_C and B_{0CR} also confirm that the magnetic grain-sizes in FA are finer than those in BA.
237 Hematite, which usually results in flat, fat loops, often not saturated, seems absent or, at least,
238 occurs at low concentrations that do not affect the shape of hysteresis curves. The fact that hematite
239 is 200 times less susceptible to magnetisation further supports this observation.

240 **3.4.1 Analysis of FORC distribution**

241 First order reversal curve (FORC) diagrams provide further information from hysteresis loops
242 that is unavailable from standard measurements. A FORC diagram is calculated from a suite of
243 partial hysteresis curves, which are measured by saturating a sample with a large positive field
244 followed by a step-wise decreasing reversal field [41]. FORC diagrams for both BA and FA
245 samples (Fig. 4) show a strong coercivity peak around 10 mT and a strong interaction fields (H_u)
246 spreading asymmetrically to high coercivities (± 80 mT BA; ± 40 mT FA), signifying a prevalent
247 ferro(i)magnetic component. A broad, not well-defined, central ridge with a long tail along the H_c
248 axis up to 100-150 mT characterises BA and FA samples and is indicative of the coexistence of
249 hard magnetic phases. Asymmetry and negative regions are commonly seen in FORC diagrams of
250 MSWI ashes. The origin of asymmetry and negative regions is ascribable to an artefact of the fitting
251 procedure, the presence of hard magnetic phases (hematite, sulphates/sulphides, and carbonates), or
252 magnetostatic interactions. This observation suggests that a hard phase is well mixed with a softer

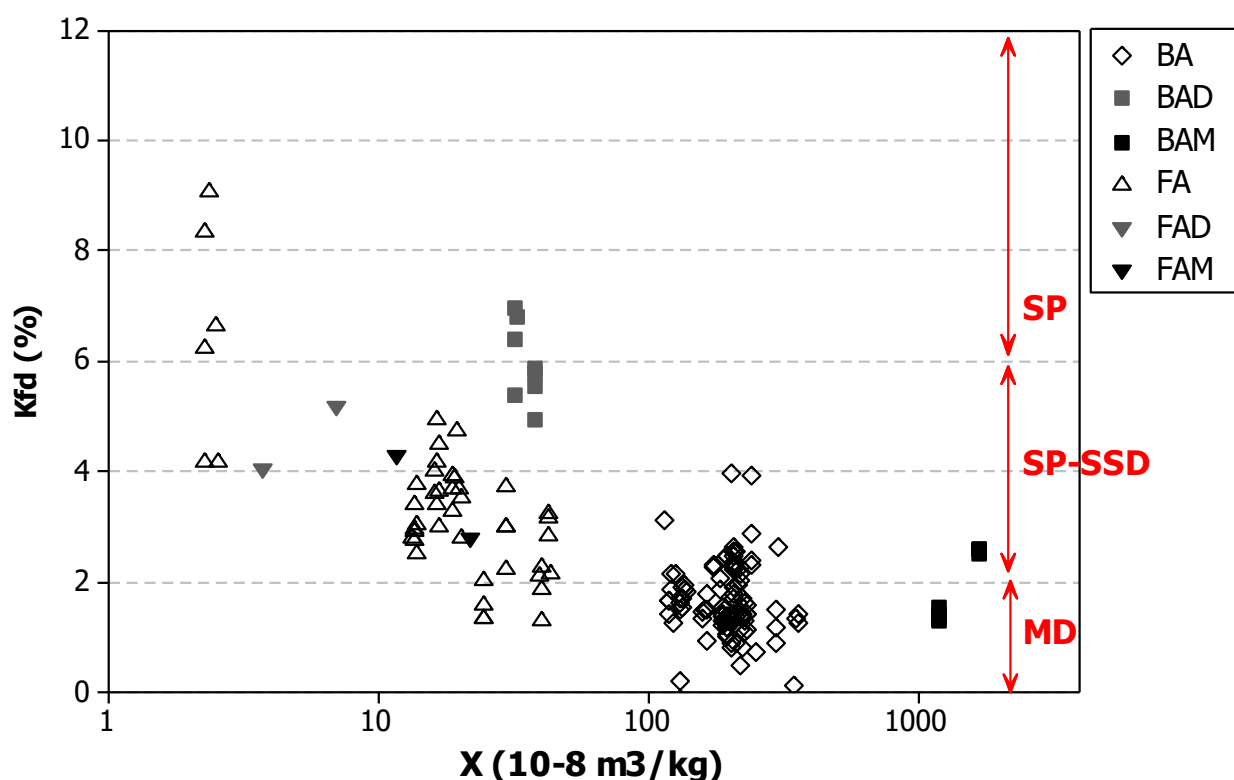
253 phase like magnetite: the overall FORC distributions are likely a result of homogeneous mixtures of
254 different mineralogical phases, which overlap and combine to give a single distribution [42]. All the
255 FORC distributions are representative of a PSD magnetic assemblage, therefore with transitional
256 behaviour between true MD and SD grains. The presence of closed contours near the maximum
257 distribution peaks further points to fine SD and PSD grains as the prevalent magnetic fraction. The
258 FORC diagram representative for BA materials (Fig. 4a) is typical of PSD materials and approaches
259 the reference diagrams for synthetic aluminous iron oxides and those for natural sulphidic
260 sediments [43]. The FA materials express a similar FORC distribution which is, however,
261 transitional towards SP materials (compare FORC distribution for SP greigite [43]).



262 **Fig. 4** - First-order reversal curve (FORC) diagrams for representative samples of BA (a), FAE (b), and FAU
263 (c). The FORC diagrams are computed using FORCinel software [44] that allowed the processing with
264 optimum smoothing factor (SF), magnetic drift and first point artefact corrections.

265 **3.5 Magnetic susceptibility of MSWI ashes**

266 Fig. 5 plots the mass specific magnetic susceptibility (χ) and its frequency dependence (κ_{fd})
267 (see SI). The susceptibilities clearly cluster BA and FA samples. The magnetic extracts (closed
268 symbols in Fig. 5) are also separated accordingly, even though the magnetic separation is less
269 efficient for FA than BA as suggested by the spread in the χ ranges. The average χ values of BA
270 samples range $179\text{-}226 \times 10^{-8} \text{ m}^3/\text{kg}$, being the highest χ value $362 \times 10^{-8} \text{ m}^3/\text{kg}$. The FA samples
271 show χ values about one order of magnitude lower than those for BA, averaging $20.2 \times 10^{-8} \text{ m}^3/\text{kg}$.
272 These data are in agreement with previous magnetic measurements on MSWI ashes [27] and partly
273 lie within the range of χ values for MSW landfill leachates ($64\text{-}970 \times 10^{-8} \text{ m}^3/\text{kg}$) [25] and other
274 incineration residues such as coal fly ashes ($306\text{-}4804 \times 10^{-8} \text{ m}^3/\text{kg}$) [17, 18]. The χ measurements
275 of MSWI ashes reported here are consistent with those of sediments near Fe-smelters ($200\text{-}600 \times$
276 $10^{-8} \text{ m}^3/\text{kg}$) [14] as well as they closely agree with the χ values of residues after lignite burning,
277 cement dust, and coke dust ($579, 146, 356 \times 10^{-8} \text{ m}^3/\text{kg}$ on average, respectively) [18]. The FA
278 samples from bag filters, especially FAS, experience low susceptibilities ($2.3\text{-}14 \times 10^{-8} \text{ m}^3/\text{kg}$) as a
279 likely consequence of low iron contents in those materials. The intensities of the measured
280 susceptibility are proportional to the average iron contents determined by XRF (Table S.4),
281 indicating Fe-bearing minerals are chief carriers of the magnetic signal. Also, the lower
282 susceptibilities are ascribable to a higher proportion of total iron contained in paramagnetic
283 minerals (this mainly pertains the FA samples).



284

285 **Fig. 5** Frequency dependent susceptibility (κ_{fd} %) vs. mass specific magnetic susceptibility (χ) for BA and FA
 286 samples, including their magnetic extracts (where the suffix M= magnetic; D= (more) diamagnetic).
 287 Magnetic state domains boundaries as defined by Dearing et al. [9].

288 A characteristic feature of MSWI ashes is the relatively high percentages of κ_{fd} , exceeding the
 289 2% in most of the measures and reaching peaks greater than 8% for a few samples, in agreement
 290 with the first measures of magnetic susceptibility on MSWI ashes [27]. The BA samples (1.7 κ_{fd} %
 291 on average) show lower κ_{fd} values with respect to the FA ones (3.6 κ_{fd} % on average) whence
 292 maxima are recorded for the samples that belong to the FAS category. Values of κ_{fd} % similar to
 293 those observed for MSWI samples are quite uncommon amongst anthropogenic materials. For
 294 example, magnetic measurements on solid industrial end-products from thermoelectric power plants
 295 and steelworks resulted in κ_{fd} % averages narrowly at, or below, the 2% threshold [16]. Coal fly
 296 ashes despite high χ averages, experience lower κ_{fd} % values compared to those from MSWI FA
 297 [45]. Nonetheless, a wide range of materials of both geogenic and anthropogenic origin such as
 298 Chinese loess, pedogenetic soil horizons, urban topsoils, street dust, and urban particulate matter,
 299 have levels of κ_{fd} comparable to MSWI samples [7, 12, 46]. Many authors reported that these
 300 materials characterised by a high κ_{fd} parameter have abundant SP-sized grains. Fig. 5 shows that
 301 more than 50% BA samples are MD-dominated, while the remaining BA lie within the SP-SSD
 302 region. It is worth noting that the BA (more) diamagnetic extracts experience higher κ_{fd} % than the

303 magnetic ones, indicating a potential contribution of SP grains in the BA materials. Conversely, the
304 most of FA is in the SP-SSD region, and some are in a SP state. According to the semi-quantitative
305 model by Dearing et al. [9], MSWI samples result in relatively high contents (>10% on mass
306 weight) of SP particles overreaching the 2% κ_{fd} threshold in the majority of samples. Anthropogenic
307 magnetic minerals are usually large magnetic grains in a MD state, but the χ_{fd} parameter for MSWI
308 ashes likely indicates admixtures of SP and coarser non-SP grains, being the latter component
309 MD/PSD-dominated.

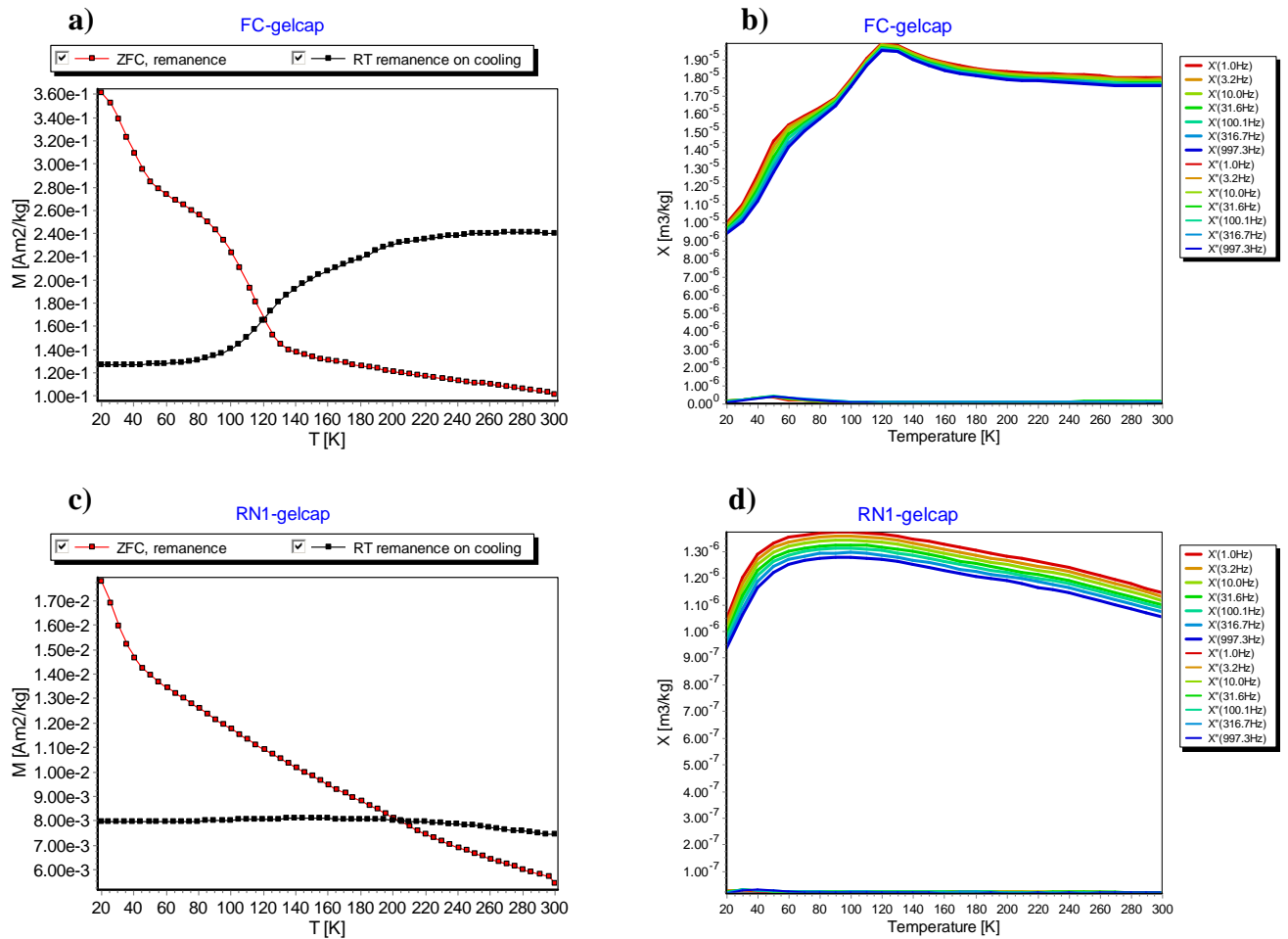
310 A contribution of the SP fraction derived from the κ_{fd} parameter can be misinterpreted for
311 rather varying mineralogical assemblages and needs to be further supported by more robust means,
312 for example by temperature-dependent data. We attempt to quantify the SP fraction of MSWI ashes
313 in a section sotto, where a comparison with other techniques such as low-temperature
314 remanence/susceptibility measurements [47, 48] is provided.

315 ***3.6 Magnetic Properties Measurement System (MPMS)***

316 Selected BA and FA samples were measured using the MPMS to probe in detail magnetic
317 mineralogy and eventual SP behaviour. In Fig. 6, low-temperature remanence curves are obtained
318 by first imparting a 2.5 T SIRM at room temperature (RTSIRM) and measuring during zero-field
319 cooling (ZFC) to 20 K (RT remanence on cooling), and then imparting a 2.5 T SIRM at low
320 temperature (LTSIRM) and measuring while zero-field heating back to room temperature from 20
321 K (ZFC, remanence). Further details regarding the acquisition procedure are provided elsewhere
322 [49]. The measured sequences show magnetite-like shapes for most of MSWI samples.
323 Nonetheless, the low-temperature remanence curves of BA and FA samples have distinct shapes in
324 agreement with the preliminary observation reported in [31]. The BA samples systematically show
325 a dramatic loss of remanence between 100 K and 130 K during zero-field cooling (Fig. 6a). This
326 drop, associated with the isotropic point and the Verwey transition, confirms that magnetite is the
327 main remanence carrier in BA material. This feature is recognisable for the reference curves of
328 coarse-grained magnetite albeit the drop of remanence in pure MD magnetite is very sharp and
329 narrower at 120 K. Most probably, the observed curves for BA samples are characteristic of
330 mixtures of coarse (e.g., MD) and fine (e.g., SD/PSD/SP) grains and adhere, for example, to
331 reference curves of pozzolanic materials [50]. BA curves display an additional small drop on
332 cooling at about 190 K (Fig. S.4) that may be due to nano hematite [51]. Conversely, the ZFC
333 LTSIRM warming curves of FA samples show a steep decrease at very low temperatures and
334 monotonically decrease after ~40 K. The room-temperature remanence shows a flat trend, which is
335 expressed by 90% of the FA samples in this study (the remaining 10% shows almost the same

336 behaviour of BA samples). The Verwey transition in FA samples is not clear probably due to the
337 presence of oxidised/impure magnetite or unblocking of SP grains. Overall, the behaviour of the
338 remanence for FA samples suggests the presence of finer grains than those occurring in BA
339 materials as well as a crowd of minerals much more oxidised (or hydrated). The measured curves of
340 FA samples resemble those of maghemite or pozzolanic ash.

341 The Verwey transition typically occurs at ~120 K in stoichiometric magnetite, but the
342 observed Verwey transitions for MSWI ashes occur over a broad temperature range (i.e., 110-130
343 K), indicating nonstoichiometry (see also Fig. 6) and the presence of grains partly oxidised (i.e.,
344 maghemitization). According to the first derivatives of the ZFC-FT curves (Fig. S.4) and the
345 remanence changes associated with the Verwey transitions, it is clear that magnetite is less oxidised
346 in BA than FA. Other phase transitions occur in BA and FA samples over characteristic temperature
347 ranges, which are liable of the remanence carried by different minerals. Phase transitions of FA
348 samples are less clear than those of BA samples, but still present (Fig. 6a and c). A phase transition
349 at about 30 K on ZFC curves is always present and visible both in BA and FA samples. This might
350 indicate either i) the presence of siderite (FeCO_3) that experiences a magnetic transition at ~38 K or
351 ii) the Besnus transition (30-34 K) diagnostic of monoclinic pyrrhotite, despite it is not visible in the
352 RTSIRM cooling curves, or iii) most likely, an effect due to a poorly-understood electronic
353 relaxation phenomenon in pure and oxidised magnetite at that T. The RT curves of both BA and FA
354 sample reveal weak magnetic transitions at ~260 K and ~190 K (see also Fig. S.4) probably
355 corresponding to the Morin transition for $\alpha\text{-Fe}_2\text{O}_3$ hematite and nanohematite, respectively.
356 Measurements of AC susceptibility by MPMS (Fig. 6b and d) support a significant contribution of
357 SP grains especially in FA materials. FA samples show larger frequency dependence than BA and
358 the temperature of the peak in both in-phase and out-of-phase susceptibility (X' and X'' in Fig. 6),
359 which corresponds to the blocking temperature, is shifted towards lower temperature (~30 K for
360 FA; ~50 K for BA). Both in-phase (X') and out-of-phase (X'') susceptibilities are one order of
361 magnitude higher in BA than in FA. The increased amplitudes in BA samples can be due to either
362 one or a combination of the following factors: i) conductive eddy currents, indicating the presence
363 of native metals or graphite; ii) high contents of pyrrhotite, hematite, iron or titanomagnetite; iii)
364 significant SP/SD presence [19]. The MPMS measurements confirm the presence of a significant
365 population of SP grains in FA samples, and a less significant but still detectable SP population in
366 BA samples. In general, mixed mineral assemblages encompassing impure (titano)magnetite,
367 (titano)hematite, ilmenite, pyrrhotite, and native metals are characteristic of these anthropogenic
368 materials and may conceal the real SP contribution.

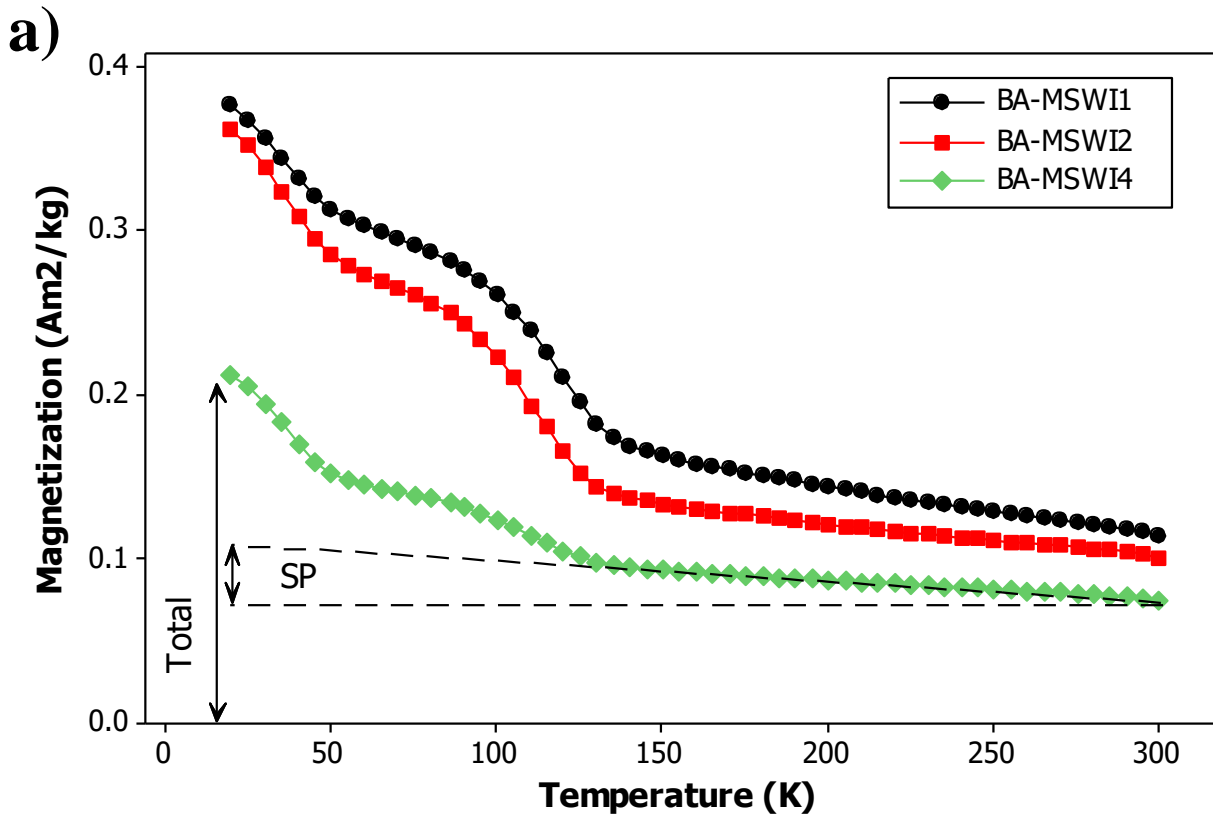


369 **Fig. 6** MPMS measurements of representative BA sample (above) and FA sample (below). Low-temperature
 370 remanence curves (a, c) during zero-field cooling to 20 K (RT remanence on cooling) and on heating
 371 back to room temperature (ZFC, remanence). AC susceptibility (b, d) is measured at 7 different
 372 frequencies and in fixed field amplitude as a function of temperature; both in-phase (X') and out-of-
 373 phase (X'') susceptibility are displayed.

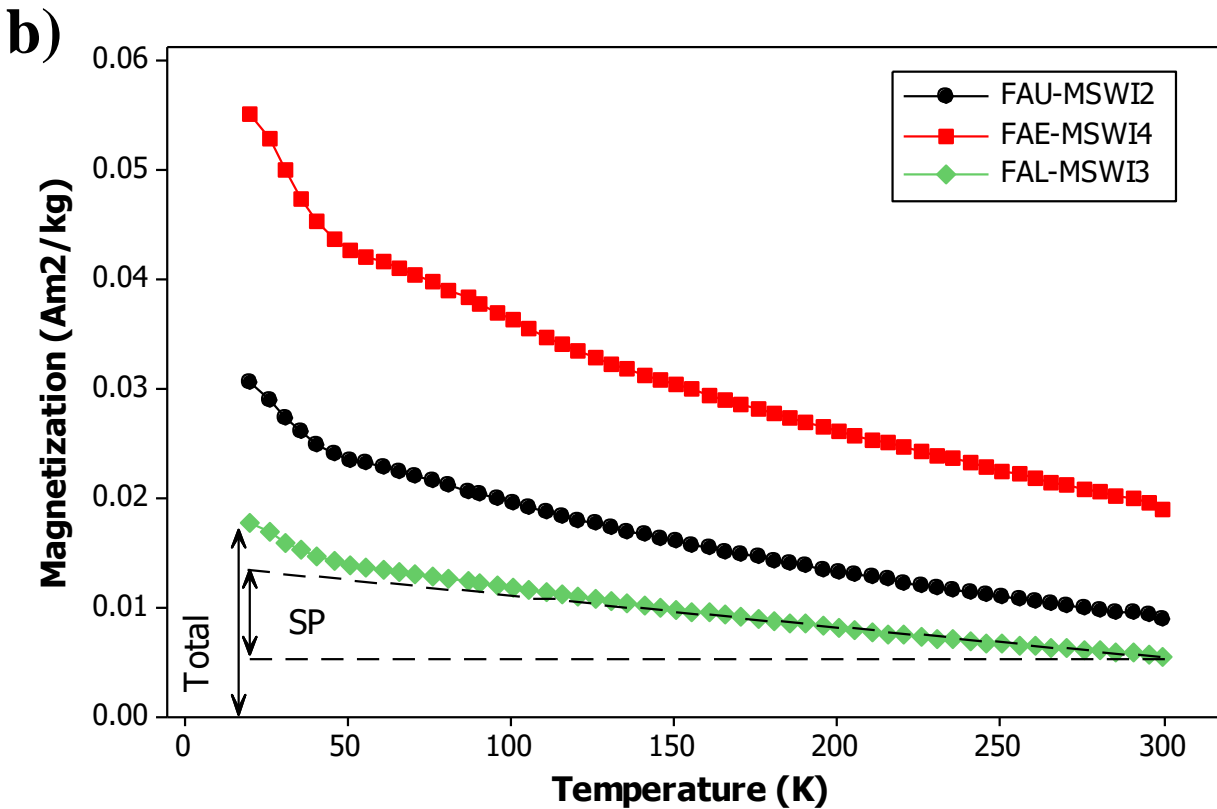
374 3.6.1 Estimation of the SP fraction

375 The low-temperature remanence curves in Fig. 6 display a steep decay between 20 and 40 K
 376 for both samples and another steep drop between 100 and 120 K for the BA sample, superimposed
 377 on a smooth monotonic decrease towards ambient temperatures, which may be attributed to the
 378 progressive unblocking of the SP population. Other evidence of a SP contribution in both BA and
 379 FA obtained from previous sections (e.g., the χ_{fd} parameter, the hysteresis properties) adds to this
 380 observation. Although a magnetic method that provides a quantitative measure of the amount of SP
 381 grains in environmental or anthropogenic sample materials doesn't exist, Banerjee *et al.* (1993)
 382 proposed a method based on thermal unblocking of LTSIRM for a quantitative estimate of the SP
 383 fraction ($d < 30$ nm) of magnetite. By using the same approach, we tried to measure the real
 384 contribution of SP grains on the magnetic response. The Fig. 7 attempts to compare low-
 385 temperature thermal demagnetization of the SIRM for several BA and FA samples and to apply the

386 graphical interpretation technique. The general loss of remanence between 20 K and 300 K
387 indicates a significant presence of SP nanoparticles; while the slightly different slope amongst the
388 samples in Fig. 7 suggests a small variation in grain-size distribution of magnetic particles. The
389 contribution to the remanence of SP grains can be determined by subtracting both the value of the
390 thermally-stable 300 K remanence (from the whole curve) and the remanence lost during the T_V
391 (the specific temperature value of T_V was extrapolated from the first derivative of the remanence
392 curve for each sample). The values for SP content obtained using the graphical method point to a SP
393 fraction in the range of 16-22% in BA samples and a 25-31% SP fraction is found in FA samples.
394 Although Fig. 7a and b show the simultaneous presence of large and small grains in both BA and
395 FA samples, the contribution of SP grains is considerable and relatively higher in FA rather than
396 BA as argued before. Very interesting observations are the following: i) since the BA samples have
397 a lower SP fraction compared to FA samples, most of the SP grains are probably carried from the
398 combustion chamber to the APC system; ii) the largest content of SP grains is estimated in FAU,
399 which represents the material recovered from the first section of filtration [33], suggesting that most
400 of the SP grains are not caught by the subsequent steps and are thus released in the atmosphere. In
401 addition, the values for SP content obtained exploiting the ratio χ to SIRM [48] compare favourably
402 with the more reliable thermal demagnetization of low-temperature SIRM technique: SP fractions
403 lie in the range 10-35% and 26-58% for BA and FA, respectively. In this case, the increases of
404 χ /SIRM (assumed to be due to SP grains) are measured with reference to a baseline, which was
405 selected to be the lowest measured χ /SIRM value. These estimates are conservative because we
406 measured, with all probabilities, only a fraction of SP grains that survives to preserve this signal.
407 Moreover, diverse oxidation levels in BA and FA magnetic minerals translates in an artificial
408 lowering of SP/total ratio [52] and the probable presence of iron oxyhydroxides (e.g., the RT-ZFC
409 curves likely contain a signal from ferrihydrite) could result in a further underestimate of the SP
410 fraction using the low-temperature technique [48].



411



412

413 **Fig. 7** Low-temperature thermal demagnetisation of a SIRM imparted at 20 K, for representative samples of
 414 BA (a) and FA (b). Ashes deriving from different MSWI plant and different FA categories are also
 415 indicated. Note the graphical analysis according to the method of Banerjee et al. (1993).

416 4. CONCLUDING REMARKS

417 *4.1 Disentangling mixed magnetic mineral assemblages of Fe-bearing phases*

418 The high values of magnetic susceptibility (χ) of MSWI ashes (Fig. 5) and their direct relation
419 to the total iron contents (Table S.4) suggest that iron oxides are the dominant magnetic carriers,
420 irrespective of the MSWI combustor designs and heterogeneous waste feed. All the magnetic
421 measurements verified the chief role of magnetite-like phases in both BA and FA samples.
422 According to the Mössbauer analysis, the magnetite to hematite ratio is higher in BA than in FA
423 samples. The low content of magnetite in FA results in lower χ values compared to those of BA. A
424 large amount of hematite in FA reasonably depends on the lower temperature profile and the
425 different oxygen pressure within the APC system. A contribution of hard magnetic phases and
426 paramagnetic minerals has been proven for both BA and FA samples, but the ferro(i)magnetic
427 component of BA is found to be overwhelming. The strong magnetic signal of BA samples likely
428 depends on iron oxides sourced from waste metal fragments that were assimilated by melting and
429 later re-crystallized during incineration and quenching. Conversely, the chemical additives used in
430 the APC system virtually dilute the ferro(i)magnetic component of FA. The magnetic spinels found
431 in MSWI ashes, especially those occurring in FA, are ferrite according to the temperature-
432 dependent data. Ferrimagnetic intermediate titanohematite and titanomagnetite can occur in FA and
433 BA, respectively (FeO-TiO₂-Fe₂O₃ ternary diagram in Fig. S.5), and add to the overall magnetic
434 response.

435 Nonstoichiometry is pervasive for minerals in MSWI ashes as suggested by the MPMS
436 transition temperatures. The simultaneous presence of magnetite, maghemite, and hematite
437 confirmed by rock magnetic measurements and wüstite inferred by the XRD analysis, emphasises
438 complex pathways of mineral formation. Intermediate phases with iron vacancies and substitution
439 of di- and tri-valent metals occur in BA and FA sample from MSWI, as argued for other
440 anthropogenic materials [15, 45]. Many magnetic measurements may infer hard magnetic phases
441 such as greigite, monoclinic pyrrhotite, antiferromagnetic oxides, and siderite, but they are hardly
442 confirmed. The Mossbauer analysis apparently detects magnetite and hematite alone, but the
443 following factors may have concealed other Fe-bearing minerals: the thermal relaxation effect,
444 overlaps of (sub)doublets, anomalies of the hyperfine field of Bhf, and a considerable amorphous
445 phase. The coarse resolution of the XRD analyses coupled with the presence of many mineralogical
446 phases at elevated concentrations prevented a comprehensive identification of minerals in our
447 samples. Hysteresis properties and temperature-dependent phase transitions ought to represent,
448 other than magnetite, maghemite or sulphur minerals; sulphides and sulphates are naturally

449 incompatible minerals, but they may coexist in MSWI residues in complex phase equilibrium or
450 perhaps disequilibrium. For example, pyrrhotite is an intermediate product of the chemical pathway
451 to pyrite formation and arises in reductive conditions in a wide temperature window (ca. 300-1100°
452 C; [18]) which roughly corresponds to that encountered in different stages of a MSWI system.
453 Sulphide minerals, especially those of the pyrite group, may end up in the municipal solid waste
454 feed as they are essential for various applications such as, cathode material in Li-batteries,
455 semiconductors, and photovoltaic solar panels. Besides iron oxides, care should also be given to
456 sulphur-related pollution which is an important factor of risk associated with lung cancer and
457 cardiopulmonary mortality [2].

458 In summary, the integration of information from our magnetic and non-magnetic techniques
459 leads us to conclude that the dominant magnetic carrier in our samples is magnetite and its
460 intermediate/impure forms (e.g., titanomagnetite, maghemite, titanohematite, and ferrite), while
461 sulphates/sulphides (monoclinic pyrrhotite, magnetic Fe³⁺ sulphate) and carbonates are important
462 ancillary magnetic carriers. This might strongly affect the magnetic properties of MSWI ashes and,
463 in turn, prevent an efficient use of many fundamental magnetic plots that have to be regarded with
464 caution.

465 ***4.2 Anthropogenic pollution and SP nanoparticles***

466 A distinct magnetic signature characterises BA and FA generated in MSWI plants as it was
467 predicted in a preliminary study [31]. Relatively high values of χ and κ_{FD} are characteristic
468 parameters of MSWI ashes. Measurements of the field- and temperature-dependence of induced and
469 remanent magnetisation show discernable differences between BA and FA samples. It has been
470 proven that BA and FA's magnetic properties notably differ from those of loess, sediments, or soil
471 resulting from natural processes [11] as well as other anthropogenic sources of pollution, such as
472 coal fly ashes, dust from power stations or Fe-smelters, and landfill leachates [18]. The present
473 study thus provides reference data for discriminating anthropogenic ferrimagnetic particles
474 originated from MSWI systems.

475 The most important finding is the observed SP behaviour of BA and FA materials. The κ_{FD}
476 parameter readily detected a contribution of SP particles and can be a reliable indicator for the
477 preliminary assessment of the SP potential of MSWI ashes. Indeed, measurements of frequency-
478 dependent susceptibility performed on-site can serve as a fast and cost-effective tool for monitoring
479 SP nanoparticles. The SP fraction of BA and FA materials was confirmed and semi-quantitatively
480 determined by temperature-dependent measures. The results presented above for SP concentrations

481 (Fig. 7), which provide output predictions for four national MSWI facilities, were obtained using
482 representative samples from the first half-year of waste production. A SP amount of up to 31% (for
483 FA) is alarming, but the dusty nature of MSWI ashes is well-known and routinely complicates their
484 safe management. The estimated amounts of ultrafine particles are consistent with other works that
485 revealed more than half of the FA material is submicron-sized, according to laser grain-size analysis
486 [29]. SP-sized grains in MSWI ashes are unlikely to be detected by non-magnetic techniques; in
487 fact, we suppose that the SP fraction, being associated with a population of large ferrimagnetic MD
488 particles, either occurs as a coating of MD particles, as argued for traffic-related particulate matter
489 [6], or agglomerates during re-deposition [53]. As such, SP magnetic state does not mean ultrafine
490 particles readily available to mobilization and transport. The different analytical sensitivities to
491 grain-size and mineralogy highlight the importance of combined approaches to assess the nano-
492 pollution related to SP grains in MSWI ashes. The following estimates assume the SP fraction is
493 made of discrete grains and are intended to raise awareness about potential risks and to further our
494 understanding on this particular kind of anthropogenic material. Taking the average of MSWI BA
495 and FA outputs ($3.5 \cdot 10^4$ t/a and $4.1 \cdot 10^3$ t/a, respectively [33]) and the estimated SP concentrations
496 according to Banerjee's graphical method on low-temperature demagnetization curves, we obtain a
497 SP fraction ranging 5.6-7.7 (BA) and 1.0-1.3 (FA) kilo tons/year. These figures are indicative of the
498 SP annual flow from solid ashes of a typical MSWI system and translate to $\sim 45 \cdot 10^4$ tons/year SP
499 grains (as a maximum range value) discharged every year by a medium-sized country running 50
500 MSWI plants. The overall SP contribution is likely underestimated and does not include the SP
501 fraction that is not retained by the MSWI filters and escapes in the atmosphere. Buonanno et al.
502 concluded that the ultrafine particle emission from waste incinerators is negligible and that the
503 efficiency of the filtration devices is relatively high [30]. However, their review relies on a limited
504 number of studies based on non-magnetic methods. Considering an average of $1.03 \cdot 10^5$ t/a of
505 particulate vapour escaping from the smokestack of a typical MSWI plant [33] and a conservative
506 10% SP estimate included in this particulate emission, a resulting SP fraction in the order of 10^4 t/a
507 is realistic and significant in a long-term view. We can surmise that agglomeration and clamping of
508 smaller SP grains with larger ones favour the filtration efficiency and decrease the inhalation risk.
509 Nonetheless, the SP fraction estimates stress the risk related to re-suspended dust during handling
510 and recycling processes. It was not in the scope of this study to assess the SP particulate emissions
511 via air-quality monitoring systems or whether our estimates on solid outputs are directly related to
512 the size of the MSWI facilities, system designs, or waste feed compositions, but certainly, that
513 would be the objective of future research.

514 Given these premises, it is logical that the numerous MSWI facilities producing huge amounts
515 of solid residues and particulate vapour have a significant impact on urban areas. The inhalation risk
516 related to nanoparticles from MSWI hot spots may have a severe effect locally (within 50 km
517 distance) although sulphur species could overcome larger distances [23]. As such, ultrafine
518 pollution from waste incineration may add to the general particulate pollution from a range of
519 outdoor sources (e.g., traffic) to which people are exposed. So, there is a need to calibrate the
520 current technologies towards the safer management of incineration waste and plan new monitoring
521 strategies that consider the use of magnetic methods. Alterations to the combustion process or the
522 implementation of secondary treatment technologies may render the MSWI systems more
523 environmentally secure and the MSWI ashes better suited for handling, reuse, or long-term
524 landfilling.

525 **ACKNOWLEDGMENTS**

526 The authors gratefully acknowledge the following people for their valuable assistance during
527 measurements/interpretation: Mike Jackson, Dario Bilardello, Peter Solheid, and Bruce Moskowitz
528 (Institute for Rock Magnetism – IRM, Minneapolis), Giorgio Gasparotto and Giovanni Valdré
529 (BiGeA Department – Bologna). We sincerely thank Mike Jackson (Institute for Rock Magnetism –
530 IRM, Minneapolis) for reviewing the first draft of this manuscript. Special thanks are due to the
531 Associate Editor Kevin V. Thomas for handling the manuscript, and to Aldo Winkler and three
532 anonymous referees for their helpful comments.

533 An IRM Visiting Fellowship granted to V.F. allowed performing part of this work at the
534 Institute for Rock Magnetism (IRM) at the University of Minnesota. The IRM is a US National
535 Multi-user Facility supported through the Instrumentation and Facilities program of the National
536 Science Foundation, Earth Sciences Division, and by funding from the University of Minnesota.

537 **REFERENCES**

- 538 1. W.H.O., *World Health Organization. Health effects of particulate matter. Policy implications for*
539 *countries in eastern Europe, Caucasus and central Asia.* [http://www.euro.who.int/en/health-](http://www.euro.who.int/en/health-topics/environment-and-health/air-quality/publications/2013/health-effects-of-particulate-matter.-policy-implications-for-countries-in-eastern-europe,-caucasus-and-central-asia-20132013)
540 [topics/environment-and-health/air-quality/publications/2013/health-effects-of-particulate-](http://www.euro.who.int/en/health-topics/environment-and-health/air-quality/publications/2013/health-effects-of-particulate-matter.-policy-implications-for-countries-in-eastern-europe,-caucasus-and-central-asia-20132013)
541 [matter.-policy-implications-for-countries-in-eastern-europe,-caucasus-and-central-asia-20132013.](http://www.euro.who.int/en/health-topics/environment-and-health/air-quality/publications/2013/health-effects-of-particulate-matter.-policy-implications-for-countries-in-eastern-europe,-caucasus-and-central-asia-20132013)
542 2. Pope III, C.A., Burnett, R.T., Thun, M.J., Calle, E.E., Krewski, D., Ito, K., and Thurston, G.D., *Lung*
543 *Cancer, Cardiopulmonary Mortality, and Long-term Exposure to Fine Particulate Air Pollution.*
544 *JAMA*, 2002. **287**(9): p. 1132-1141; DOI: 10.1001/jama.287.9.1132.
545 3. Maher, B.A., Ahmed, I.A., Karloukovski, V., MacLaren, D.A., Foulds, P.G., Allsop, D., . . . Calderon-
546 *Garciduenas, L., Magnetite pollution nanoparticles in the human brain.* Proceedings of the National

- 547 Academy of Sciences of the United States of America, 2016. 10.1073/pnas.16059411113; DOI:
548 10.1073/pnas.1605941113.
- 549 4. Thompson, R. and Oldfield, F., *Environmental Magnetism*. 1 ed. 10.1007/978-94-011-8036-81986,
550 London: Springer Netherlands. 228.
- 551 5. Muxworthy, A.R., Schmidbauer, E., and Petersen, N., *Magnetic properties and Mössbauer spectra of*
552 *urban atmospheric particulate matter: a case study from Munich, Germany*. Geophysical Journal
553 International, 2002. **150**(2): p. 558-570.
- 554 6. Sagnotti, L. and Winkler, A., *On the magnetic characterization and quantification of the*
555 *superparamagnetic fraction of traffic-related urban airborne PM in Rome, Italy*. Atmospheric
556 Environment, 2012. **59**: p. 131-140; DOI: 10.1016/j.atmosenv.2012.04.058.
- 557 7. Zhu, Z., Li, Z., Bi, X., Han, Z., and Yu, G., *Response of magnetic properties to heavy metal pollution in*
558 *dust from three industrial cities in China*. Journal of Hazardous Materials, 2013. **246-247**: p. 189-98;
559 DOI: 10.1016/j.jhazmat.2012.12.024.
- 560 8. Hansard, R., Maher, B.A., and Kinnersley, R.P., *Rapid magnetic biomonitoring and differentiation of*
561 *atmospheric particulate pollutants at the roadside and around two major industrial sites in the U.K.*
562 *Environmental Science & Technology*, 2012. **46**(8): p. 4403-10; DOI: 10.1021/es203275r.
- 563 9. Dearing, J.A., Bird, P.M., Dann, R.J.L., and Benjamin, S.F., *Secondary ferrimagnetic minerals in Welsh*
564 *soils: a comparison of mineral magnetic detection methods and implications for mineral formation*.
565 *Geophysical Journal International*, 1997. **130**(3): p. 727-736; DOI: 10.1111/j.1365-
566 246X.1997.tb01867.x.
- 567 10. Jordanova, N., Jordanova, D., Veneva, L., Yorova, K., and Petrovsky, E., *Magnetic Response of Soils*
568 *and Vegetation to Heavy Metal Pollutions - A Case Study*. *Environmental Science & Technology*,
569 2003. **37**: p. 4417-4424; DOI: 10.1021/es0200645.
- 570 11. Fialová, H., Maier, G., Petrovský, E., Kapička, A., Boyko, T., and Scholger, R., *Magnetic properties of*
571 *soils from sites with different geological and environmental settings*. *Journal of Applied Geophysics*,
572 2006. **59**(4): p. 273-283; DOI: 10.1016/j.jappgeo.2005.10.006.
- 573 12. Wang, X., Løvlie, R., Zhao, X., Yang, Z., Jiang, F., and Wang, S., *Quantifying ultrafine pedogenic*
574 *magnetic particles in Chinese loess by monitoring viscous decay of superparamagnetism*.
575 *Geochemistry, Geophysics, Geosystems*, 2010. **11**(10): p. n/a-n/a; DOI: 10.1029/2010gc003194.
- 576 13. Vigliotti, L., Capotondi, L., and Torii, M., *Magnetic properties of sediments deposited in suboxic-*
577 *anoxic environments: relationships with biological and geochemical proxies*. Geological Society,
578 London, Special Publications, 1999. **151**(1): p. 71-83; DOI: 10.1144/gsl.sp.1999.151.01.08.
- 579 14. Zhang, C., Qiao, Q., Piper, J.D., and Huang, B., *Assessment of heavy metal pollution from a Fe-*
580 *smelting plant in urban river sediments using environmental magnetic and geochemical methods*.
581 *Environmental Pollution*, 2011. **159**(10): p. 3057-70; DOI: 10.1016/j.envpol.2011.04.006.
- 582 15. Veneva, L., Hoffmann, V., Jordanova, D., Jordanova, N., and Fehr, T., *Rock magnetic, mineralogical*
583 *and microstructural characterization of fly ashes from Bulgarian power plants and the nearby*
584 *anthropogenic soils*. *Physics and Chemistry of the Earth, Parts A/B/C*, 2004. **29**(13-14): p. 1011-
585 1023; DOI: 10.1016/j.pce.2004.03.011.
- 586 16. Jordanova, D., Jordanova, N., and Hoffmann, V., *Magnetic mineralogy and grain-size dependence of*
587 *hysteresis parameters of single spherules from industrial waste products*. *Physics of the Earth and*
588 *Planetary Interiors*, 2006. **154**(3-4): p. 255-265; DOI: 10.1016/j.pepi.2005.06.015.
- 589 17. Lu, S.G., Chen, Y.Y., Shan, H.D., and Bai, S.Q., *Mineralogy and heavy metal leachability of magnetic*
590 *fractions separated from some Chinese coal fly ashes*. *Journal of Hazardous Materials*, 2009. **169**(1-
591 3): p. 246-55; DOI: 10.1016/j.jhazmat.2009.03.078.
- 592 18. Magiera, T., Jabłońska, M., Strzyszczyński, Z., and Rachwał, M., *Morphological and mineralogical forms*
593 *of technogenic magnetic particles in industrial dusts*. *Atmospheric Environment*, 2011. **45**(25): p.
594 4281-4290; DOI: 10.1016/j.atmosenv.2011.04.076.
- 595 19. Moskowitz, B.M., Jackson, M., and Chandler, V., *Geophysical Properties of the Near-Surface Earth:*
596 *Magnetic Properties*. 2015. In: *Treatise on Geophysics, Second Edition*: p. 139-174; DOI:
597 10.1016/b978-0-444-53802-4.00191-3.
- 598 20. Englert, N., *Fine particles and human health--a review of epidemiological studies*. *Toxicology*
599 *Letters*, 2004. **149**(1-3): p. 235-42; DOI: 10.1016/j.toxlet.2003.12.035.

- 600 21. Solaimani, P., Saffari, A., Sioutas, C., Bondy, S.C., and Campbell, A., *Exposure to ambient ultrafine*
601 *particulate matter alters the expression of genes in primary human neurons*. *Neurotoxicology*, 2016.
602 **58**: p. 50-57; DOI: 10.1016/j.neuro.2016.11.001.
- 603 22. Levy, J.I., Wilson, A.M., Evans, J.S., and Spengler, J.D., *Estimation of Primary and Secondary*
604 *Particulate Matter Intake Fractions for Power Plants in Georgia*. *Environmental Science &*
605 *Technology*, 2003. **37**(24): p. 5528-5536.
- 606 23. Lamancusa, C., Parvez, F., and Wagstrom, K., *Spatially resolved intake fraction estimates for primary*
607 *and secondary particulate matter in the United States*. *Atmospheric Environment*, 2017. **150**: p.
608 229-237; DOI: 10.1016/j.atmosenv.2016.11.010.
- 609 24. Szuskiewicz, M., Magiera, T., Kapička, A., Petrovský, E., Grison, H., and Gołuchowska, B., *Magnetic*
610 *characteristics of industrial dust from different sources of emission: A case study of Poland*. *Journal*
611 *of Applied Geophysics*, 2015. **116**: p. 84-92; DOI: 10.1016/j.jappgeo.2015.02.027.
- 612 25. Huliselan, E.K., Bijaksana, S., Srigutomo, W., and Kardena, E., *Scanning electron microscopy and*
613 *magnetic characterization of iron oxides in solid waste landfill leachate*. *Journal of Hazardous*
614 *Materials*, 2010. **179**(1-3): p. 701-8; DOI: 10.1016/j.jhazmat.2010.03.058.
- 615 26. Cernuschi, S., Giugliano, M., Ozgen, S., and Consonni, S., *Number concentration and chemical*
616 *composition of ultrafine and nanoparticles from WTE (waste to energy) plants*. *Science of the Total*
617 *Environment*, 2012. **420**: p. 319-26; DOI: 10.1016/j.scitotenv.2012.01.024.
- 618 27. Funari, V., Bokhari, S.N., Vigliotti, L., Meisel, T., and Braga, R., *The rare earth elements in municipal*
619 *solid waste incinerators ash and promising tools for their prospecting*. *Journal of Hazardous*
620 *Materials*, 2016. **301**: p. 471-479; DOI: 10.1016/j.jhazmat.2015.09.015.
- 621 28. C.P.P., *Committee for Prevention and Precaution. Municipal Solid Waste Incinerators: Risks and*
622 *Policies*, M.o.E.a.S. Development, Editor. 2004, Ministry of Ecology and Sustainable Development:
623 Paris, France. p. 1-57.
- 624 29. De Boom, A. and Degrez, M., *Belgian MSWI fly ashes and APC residues: a characterisation study*.
625 *Waste Management*, 2012. **32**(6): p. 1163-70; DOI: 10.1016/j.wasman.2011.12.017.
- 626 30. Buonanno, G. and Morawska, L., *Ultrafine particle emission of waste incinerators and comparison*
627 *to the exposure of urban citizens*. *Waste Management*, 2015. **37**: p. 75-81; DOI:
628 10.1016/j.wasman.2014.03.008.
- 629 31. Funari, V., *Magnetic characterization of solid by-products from Municipal Solid Waste Incinerators*.
630 *The IRM Quarterly*, 2016. **26**(2): p. 2-3, <http://www.irm.umn.edu/quarterly/irmq26-2.pdf>.
- 631 32. Funari, V., Braga, R., Bokhari, S.N., Dinelli, E., and Meisel, T., *Solid residues from Italian municipal*
632 *solid waste incinerators: A source for "critical" raw materials*. *Waste Management*, 2015. **45**: p.
633 206-216; DOI: 10.1016/j.wasman.2014.11.005.
- 634 33. Funari, V., Meisel, T., and Braga, R., *The potential impact of municipal solid waste incinerators ashes*
635 *on the anthropogenic osmium budget*. *Science of the Total Environment*, 2016. **541**: p. 1549-1555;
636 DOI: 10.1016/j.scitotenv.2015.10.014.
- 637 34. Eusden, J.D., Eighmy, T.T., Hockert, K., Holland, E., and Marsella, K., *Petrogenesis of municipal solid*
638 *waste combustion bottom ash*. *Applied Geochemistry*, 1999. **14**(8): p. 1073-1091; DOI:
639 10.1016/S0883-2927(99)00005-0.
- 640 35. Bayuseno, A.P. and Schmahl, W.W., *Understanding the chemical and mineralogical properties of the*
641 *inorganic portion of MSWI bottom ash*. *Waste Management*, 2010. **30**(8-9): p. 1509-1520; DOI:
642 <http://dx.doi.org/10.1016/j.wasman.2010.03.010>.
- 643 36. Bogush, A., Stegemann, J.A., Wood, I., and Roy, A., *Element composition and mineralogical*
644 *characterisation of air pollution control residue from UK energy-from-waste facilities*. *Waste*
645 *Management*, 2015. **36**: p. 119-29; DOI: 10.1016/j.wasman.2014.11.017.
- 646 37. Greenwood, N.N. and Gibb, T.C., *Mössbauer Spectroscopy*. 10.1007/978-94-009-5697-11971,
647 London: Springer Netherlands.
- 648 38. Zyryanov, V.V., Petrov, S.A., and Matvienko, A.A., *Characterization of spinel and magnetospheres of*
649 *coal fly ashes collected in power plants in the former USSR*. *Fuel*, 2011. **90**(2): p. 486-492; DOI:
650 10.1016/j.fuel.2010.10.006.

- 651 39. Gomes, S., François, M., Abdelmoula, M., Refait, P., Pellissier, C., and Evrard, O., *Characterization of*
652 *magnetite in silico-aluminous fly ash by SEM, TEM, XRD, magnetic susceptibility, and Mössbauer*
653 *spectroscopy*. Cement and Concrete Research, 1999. **29**(11): p. 1705-1711.
- 654 40. Fermo, P., Cariati, F., Pozzi, A., Demartin, F., Tettamanti, M., Collina, E., . . . Russo, U., *The analytical*
655 *characterization of municipal solid waste incinerator fly ash: methods and preliminary results*.
656 Fresenius Journal of Analytical Chemistry, 1999: p. 365 : 666–673.
- 657 41. Roberts, A.P., Pike, C.R., and Verosub, K.L., *First-order reversal curve diagrams: A new tool for*
658 *characterizing the magnetic properties of natural samples*. Journal of Geophysical Research: Solid
659 Earth, 2000. **105**(B12): p. 28461-28475; DOI: 10.1029/2000jb900326.
- 660 42. Muxworthy, A.R., *Assessing the ability of first-order reversal curve (FORC) diagrams to unravel*
661 *complex magnetic signals*. Journal of Geophysical Research, 2005. **110**(B1); DOI:
662 10.1029/2004jb003195.
- 663 43. Roberts, A.P., Liu, Q., Rowan, C.J., Chang, L., Carvallo, C., Torrent, J., and Horng, C.-S.,
664 *Characterization of hematite (α -Fe₂O₃), goethite (α -FeOOH), greigite (Fe₃S₄), and pyrrhotite*
665 *(Fe₇S₈) using first-order reversal curve diagrams*. Journal of Geophysical Research: Solid Earth,
666 2006. **111**(B12): p. 1-16; DOI: 10.1029/2006jb004715.
- 667 44. Harrison, R.J. and Feinberg, J.M., *FORCinel: An improved algorithm for calculating first-order*
668 *reversal curve distributions using locally weighted regression smoothing*. Geochemistry, Geophysics,
669 Geosystems, 2008. **9**(5): p. 1-11; DOI: 10.1029/2008gc001987.
- 670 45. Magiera, T. and Strzyszczyk, Z., *Ferrimagnetic minerals of anthropogenic origin in Soils of some polish*
671 *national parks*. Water Air and Soil Pollution, 2000. **124**: p. 37-48.
- 672 46. Maher, B.A. and Taylor, R.M., *Formation of ultrafine-grained magnetite in soils*. Letters to nature,
673 1988. **336**: p. 368 - 370; DOI: 10.1038/336368a0.
- 674 47. Banerjee, S.K., Hunt, C.P., and Liu, X.-M., *Separation of local signals from the regional*
675 *paleomonsoon record of the chinese loess plateau: a rock-magnetic approach*. Geophysical
676 Research Letters, 1993. **20**(9): p. 843-846.
- 677 48. Hunt, C.P., Banerjee, S.K., Han, J., Solheid, P.A., Oches, E., Sun, W., and Liu, T., *Rock-magnetic*
678 *proxies of climate change in the loess-palaeosol sequences of the western Loess Plateau of China*.
679 Geophysical Journal International, 1995. **123**: p. 232-244.
- 680 49. Bilardello, D. and Jackson, M., *What do the Mumpies do?* The IRM Quarterly, 2013. **23**(3): p. 1-16,
681 <http://www.irm.umn.edu/quarterly/irmq23-3.pdf>.
- 682 50. Jackson, M., Sagnotti, L., Rochette, P., and Solheid, P., *Maintaining Standards III: Pozzolana Cement*
683 *cross-calibration samples available*. The IRM Quarterly, 2003. **13**(3): p. 1-12.
- 684 51. Özdemir, Ö., Dunlop, D.J., and Berquó, T.S., *Morin transition in hematite: Size dependence and*
685 *thermal hysteresis*. Geochemistry, Geophysics, Geosystems, 2008. **9**(10): p. 1-12; DOI:
686 10.1029/2008gc002110.
- 687 52. Smirnov, A.V. and Tarduno, J.A., *Estimating superparamagnetism in marine sediments with the time*
688 *dependency of coercivity of remanence*. Journal of Geophysical Research: Solid Earth, 2001.
689 **106**(B8): p. 16135-16143; DOI: 10.1029/2001jb000152.
- 690 53. He, X., Mitrano, D.M., Nowack, B., Bahk, Y.K., Figi, R., Schreiner, C., . . . Wang, J., *Agglomeration*
691 *potential of TiO₂ in synthetic leachates made from the fly ash of different incinerated wastes*.
692 Environmental Pollution, 2017. **223**: p. 616-623; DOI: 10.1016/j.envpol.2017.01.065.

693

694